BNL-229268-2025-JAAM

CUDO: closed-form universal dwell-time optimization for computer-controlled optical surfacing

T. Wang

To be published in "Optics Express"

December 2025

Photon Sciences

Brookhaven National Laboratory

U.S. Department of Energy

USDOE Office of Science (SC), Basic Energy Sciences (BES). Scientific User Facilities (SUF)

DISCLAIMER

Research Article | Vol. 33, No. 24 / 1 Dec 2025 / *Optics Express* 50201

Optics EXPRESS

CUDO: closed-form universal dwell-time optimization for computer-controlled optical surfacing

Tianyi Wang,[1,*,†] **Lei Huang,**[1,†] **Xiaolong Ke,**[2,†] **Yingnan Ma,**[2,†] **Yiming Zhang,**[3] **Ryan Luu,**[4,5] **Vipender Negi,**[4] **Corey Austin,**[1] **Heejoo Choi,**[4,5] **Hyukmo Kang,**[4,5] **Daewook Kim,**[4,5,6] **and Mourad Idir**[1]

[1] *National Synchrotron Light Source II (NSLS-II), Brookhaven National Laboratory, P.O. Box 5000, Upton, NY 11973, USA*
[2] *School of Mechanical and Automotive Engineering, Xiamen University of Technology, 600 Ligong Road, Jimei District, Xiamen 361024, China*
[3] *School of Information Engineering, Hainan Technology and Business College, 2 Wentan Road, Guoxing Avenue, Meilan District, Haikou 570203, Hainan, China*
[4] *Wyant College of Optical Sciences, University of Arizona, 1630 E. University Blvd., P.O. Box 210094, Tucson, AZ 85721-0094, USA*
[5] *Large Binocular Telescope Observatory, University of Arizona, Tucson, AZ 85721, USA*
[6] *Department of Astronomy and Steward Observatory, University of Arizona, 933 N. Cherry Ave., Tucson, AZ 85721, USA*
[†] The authors contributed equally to this work.
[*] *tianyi@bnl.gov*

Abstract: Precision optical figuring demands fast and accurate dwell time optimization to reach nanometer- and sub-nanometer-level accuracy in next-generation optical systems. We introduce CUDO (closed-form universal dwell-time optimization), the first, to the best of our knowledge, unified closed-form analytical framework that supports both function-form and matrix-form dwell time models in computer-controlled optical surfacing (CCOS). In contrast to traditional methods, which rely on iterative optimization and hyperparameter tuning, our framework derives direct analytical solutions with no adjustable parameters. This approach unifies the solution principles of existing methods within a single mathematical model, delivering three key advantages: (1) accuracy on par with, or superior to, iterative solvers, (2) substantial reduction in computation time, and (3) numerical robustness. Comparative studies with prior art confirm that closed-form solutions achieve equivalent residual error while removing runtime bottlenecks. By simplifying the implementation and enabling real-time, scalable deployment, CUDO establishes a practical foundation for future deterministic fabrication of large-aperture and high-performance optics.

1. Introduction

As the performance demands of modern optical systems continue to rise, particularly in fields such as space exploration [1,2], extreme ultraviolet (EUV) lithography [3,4], and synchrotron and free-electron laser imaging [5,6], the need for ultra-precision high-end optics has grown substantially. These applications increasingly require nanometer- or sub-nanometer-level figure accuracy, pushing the limits of current fabrication and metrology technologies. In this context, computer-controlled optical surfacing (CCOS) techniques [7–9], such as ion beam figuring (IBF), have become essential for achieving the necessary optical specifications.

A central challenge in CCOS is the accurate and efficient computation of the dwell time map, which determines how long the machine tool (e.g., fluid jet or ion beam) should remain at each location to achieve a desired surface shape. Mathematically, this is an ill-posed inverse

#577940 https://doi.org/10.1364/OE.577940
Journal © 2025 Received 1 Sep 2025; revised 7 Nov 2025; accepted 9 Nov 2025; published 18 Nov 2025

problem, and over the past three decades numerous numerical methods have been developed to address it [10]. These methods can be systematically classified according to their mathematical representation, that is, the function-form [11–15] and matrix-form formulations [16–21]. Among them, the Robust Iterative Fourier Transform Algorithm (RIFTA) [14] is a function-form method that employs thresholded inverse filtering-based deconvolution and automates threshold selection using a Nelder-Mead optimization strategy to suppress noise and minimize total dwell time. Robust Iterative Surface Extension (RISE) [15] builds on RIFTA by introducing a polynomial-based surface extension to mitigate edge effects. Universal Dwell Time Optimization (UDO) [21], on the other hand, generalizes these ideas to the matrix-form setting, assuming a proportional relationship between the resampled surface error map and dwell time, with the optimal scaling determined via a pattern search algorithm. Although all three methods have demonstrated favorable trade-offs between shape accuracy, process feasibility, computational efficiency, and sampling flexibility [10], they depend on iterative solvers that are computationally expensive and lack a unified mathematical framework.

To overcome these fundamental limitations, in this work, we present CUDO (Closed-form Universal Dwell-time Optimization), the first unified closed-form analytical framework that supports both function-form and matrix-form dwell time models and analytically subsumes the core solution process of RIFTA, RISE, and UDO. By reformulating the underlying optimization problem, we derive a direct, non-iterative solution that eliminates the need for numerical optimization while preserving, or even enhancing, the accuracy of the original methods. The framework applies to both function-form models, where dwell time and surface error maps are defined on a shared spatial grid, and matrix-form models, where dwell points are arbitrarily distributed and independent of the measurement grid. This unified solution enables significant computational acceleration and broadens applicability across a wide range of CCOS configurations, from simulation-based design to real-time fabrication. The main contributions of CUDO are:

- A unified closed-form mathematical framework that analytically generalizes RIFTA, RISE, and UDO;
- Full support for both function-form and matrix-form dwell time models, enabling seamless application across different CCOS implementations;
- Closed-form solutions that deliver accuracy on par with or superior to existing optimization-based approaches;
- Drastic reductions in computation time, facilitating scalable and real-time optical figuring for high-resolution, large-aperture systems.

The remainder of this paper is organized as follows. Section 2 reviews the dwell time convolution model and highlights the distinction between function-form and matrix-form formulations. Section 3 details the derivation of the unified closed-form framework and demonstrates how it generalizes existing state-of-the-art methods. Section 4 presents numerical and experimental validation, including comparisons of accuracy, runtime, and total dwell time under synthetic and practical conditions. Section 6 provides information on the performance and limitations of the unified model, along with its practical implications. Finally, Section 7 concludes with a summary and future directions.

2. Function-form and matrix-form dwell time modeling

In computer-controlled optical surfacing (CCOS), material removal is typically performed using sub-aperture tools, such as compliant polishing pads, ion beams, and fluid jets. These tools have a localized, spatially confined influence on the surface, which allows for fine correction of optical figure errors but also requires precise control of their movement and dwell duration.

Optics EXPRESS

The fundamental relationship between the tool's motion and the resulting surface modification is governed by a spatial convolution model, which describes how the cumulative influence of the tool applied along a spatially varying trajectory leads to material removal. In discrete form, this model is expressed as

$$z(\mathbf{x}_j) = (\mathrm{TIF} * t)\,[\mathbf{x}_j] = \sum_{i=0}^{N_t-1} \mathrm{TIF}(\mathbf{x}_j - \mathbf{u}_i)t(\mathbf{u}_i) \tag{1}$$

where $z(\mathbf{x}_j)$ is the material removal at the measurement coordinate $\mathbf{x}_j = \left(x_j, y_j\right)$ for $j = 0, 1, \ldots, N_z-1$ with N_z being the number of surface sampling points, TIF is the Tool Influence function (TIF), $t(\mathbf{u}_i)$ is the dwell time at the dwell location $\mathbf{u}_i$, and N_t is the number of dwell points. When the the desired removal (or residual surface error) is specified as $z_e(\mathbf{x}_j)$, the corresponding dwell time distribution $t(\mathbf{u}_i)$ can be estimated through deconvolution of Eq. (1).

When the dwell locations $\mathbf{u}_i$ and surface sampling points $\mathbf{x}_j$ share the same spatial sampling, i.e., the dwell time and surface error maps are defined over identical coordinates, the convolution in Eq. (1) degenerates to a standard two-dimensional (2D) convolution. In this case, function-form methods such as RIFTA [14] and RISE [15] can be efficiently applied, typically using Fourier transform-based acceleration [10]. In contrast, when dwell points are defined along arbitrary tool path or nonuniform grids, e.g., as determined by raster or spiral tool paths [21], the dwell time must be modeled as a set of discrete values evaluated at specific coordinates $\mathbf{u}_i$]. In such cases, the convolution in Eq. (1) remains as a summation and is more naturally expressed in matrix form:

$$\underbrace{\begin{pmatrix} z_{e_0} \\ z_{e_1} \\ \vdots \\ z_{e_{N_z-1}} \end{pmatrix}}_{\mathbf{z}_e} = \underbrace{\begin{pmatrix} \mathrm{TIF}_{0,0} & \mathrm{TIF}_{0,1} & \ldots & \mathrm{TIF}_{0,N_t-1} \\ \mathrm{TIF}_{1,0} & \mathrm{TIF}_{1,1} & \ldots & \mathrm{TIF}_{1,N_t-1} \\ \vdots & \vdots & \vdots & \vdots \\ \mathrm{TIF}_{N_z-1,0} & \mathrm{TIF}_{N_z-1,1} & \ldots & \mathrm{TIF}_{N_z-1,N_t-1} \end{pmatrix}}_{\mathbf{R}} \underbrace{\begin{pmatrix} t_0 \\ t_1 \\ \vdots \\ t_{N_t-1} \end{pmatrix}}_{\mathbf{t}}, \tag{2}$$

where $\mathbf{z}_e \in \mathbb{R}^{N_z}$ is the vectorized surface error map, $\mathbf{t} \in \mathbb{R}^{N_t}$ is the dwell time vector, and $\mathbf{R} \in \mathbb{R}^{N_z \times N_t}$ is a matrix whose columns contain shifted and sampled versions of the TIF centered at each dwell point.

The choice between function-form and matrix-form models has significant implications for both algorithmic design and physical implementation. Function-form approaches are well suited for idealized or raster-based tool paths with uniform sampling, offering efficient computation and straightforward implementation. In contrast, matrix-form approaches are essential when tool paths are predefined or irregular (e.g., random [22] and spiral [23] tool paths), as is common in practical optic polishing systems. These models support arbitrary spatial configurations but typically involve greater computational cost and memory usage. Therefore, a unified framework capable of encompassing both modeling paradigms is essential for enabling robust and scalable dwell time optimization across diverse CCOS platforms.

3. Unified closed-form framework

In this section, we develop CUDO, a universal closed-form framework for dwell time optimization that generalizes existing approaches while offering significant gains in interpretability, generality, and computational efficiency. We begin by reviewing the core strategies and limitations of three state-of-the-art algorithms, RIFTA [14], RISE [15], and UDO [21], that have shaped prior work in function-form and matrix-form dwell time modeling. We then introduce a parametric polynomial formulation in the matrix-form setting, where dwell time is expressed as a nonlinear function of the target removal profile. This representation enables an analytical least-squares solution that eliminates the need for iterative optimization. We further show that the function-form model arises as a special case of the matrix formulation when the surface measurements and dwell grids coincide. Finally, we analyze the theoretical implications of the proposed model, including its robustness, smoothness, and ability to unify and extend the behaviors of existing methods.

3.1. Prior approaches to dwell time modeling

Several methods have been developed to address the inverse problem of dwell time estimation in CCOS, with representative examples including RIFTA, RISE, and UDO. These methods differ in their mathematical formulations, numerical solvers, and sampling assumptions, but all achieve the best trade-off between accuracy, process efficiency, smoothness, and computational efficiency, as quantitatively benchmarked in a recent review [10].

RIFTA [14] is a function-form method that assumes uniform spatial sampling between dwell points and surface measurements. It formulates the inverse problem as a deconvolution in the frequency domain, leveraging the Fast Fourier Transform (FFT) for efficient computation. To suppress high-frequency noise amplification during inverse filtering, RIFTA introduces a thresholding mechanism, defined as

$$t = \mathcal{F}^{-1}\left[\frac{Z_e(\omega)}{R(\omega)}\right], \tag{3}$$

where $\mathcal{F}^{-1}$ denotes the inverse of FFT, $Z_e(\boldsymbol{\omega})$ is the Fourier transform of the target removal map $z_e(\mathbf{x})$, and $\bar{R}(\boldsymbol{\omega};\alpha)$ is the thresholded spectrum of the TIF $r(\mathbf{x})$, parameterized by a regularization threshold α with

$$\bar{R}(\omega;\alpha) = \begin{cases} R(\omega), & |R(\omega)| > \alpha \\ \alpha, & \text{otherwise} \end{cases}.$$

This threshold is not manually tuned but optimized automatically via the Nelder–Mead simplex algorithm with the merit function:

$$\hat{\alpha} = \min_{\alpha} \ \mathrm{RMS}\left\{z_e(\mathbf{x}) - r(\mathbf{x}) * \mathcal{F}^{-1}\left[\frac{Z_e(\omega)}{\bar{R}(\omega;\alpha)}\right]\right\}_{CA}, \tag{4}$$

where $\{\cdot\}_{CA}$ indicates evaluation restricted to the clear aperture only. The use of FFT makes this method computationally efficient in each optimization iteration, and a total dwell time minimization scheme is integrated into the algorithm to enhance the process efficiency. Together, these features enable RIFTA to achieve minimal estimated residual error while reducing the overall processing time, offering a key advantage over traditional methods [10]. However, the non-convexity of the threshold optimization can lead to a significant runtime overhead when the initial guess is far from optimal. Furthermore, RIFTA is inherently limited to raster-based sampling and remains sensitive to edge effects and measurement noise, which may impact its robustness in practical implementations.

RISE [15] enhances RIFTA by iteratively appending polynomials-based extensions to the target removal map in the clear aperture beyond its physical boundary. These extensions are designed to preserve spatial continuity, which greatly reduces the large errors along the edges of the dwell time solution. Although RISE handles edge effects better than RIFTA, it retains the core assumptions and iterative optimization structure of RIFTA.

UDO [21] generalizes the ideas of RIFTA and RISE to the matrix-form dwell time modeling, which accommodates arbitrary sampling patterns and tool paths. To avoid directly solving the ill-conditioned system in Eq. (2), UDO assumes a linear relationship between dwell time and the surface error projected onto the dwell gird as:

$$\mathbf{t} = \beta \cdot \mathbf{R}^{\mathrm{T}} \mathbf{z}_e, \tag{5}$$

where β is the proportionality constant. Similar to RIFTA, the optimal β is found through a numerical pattern search that minimize the residual Root Mean Square (RMS) error in the clear aperture as:

$$\hat{\beta} = \min_{\beta} \ \mathrm{RMS} \left\{ \mathbf{z}_e - \beta \cdot \mathbf{R}\mathbf{R}^{\mathrm{T}} \mathbf{z}_e \right\}_{CA} . \tag{6}$$

UDO extends applicability of RIFTA and RISE to nonuniform sampling, however, it remains limited by its linear model and reliance on search-based optimization.

Despite their differences, these methods share several fundamental limitations. First, all rely on non-convex optimization using direct search algorithms, such as Nelder–Mead [14,15] or pattern search [21]. These algorithms are sensitive to initialization and do not guarantee global optimality, often leading to unpredictable computation time or suboptimal solutions. Second, as highlighted in the recent benchmark study [10], all existing dwell time optimization methods, including but not limited to RIFTA, RISE, and UDO, require one or more tunable parameters, whether threshold, regularization constants, or smoothing factors. These parameters must be manually selected or optimized through additional procedures, which complicate practical deployment and limit automation. These challenges restrict the scalability, reliability, and real-time applicability of current algorithms. A summary of these comparisons is provided in Table 1. To address these challenges, we present in the following subsection a unified, closed-form analytical framework that eliminates parameter tuning and avoids iterative search altogether. This new approach generalizes the solution principles underlying RIFTA, RISE, and UDO within a single mathematical model, offering improved computational efficiency, robustness, and ease of implementation.

Table 1. Comparison of existing dwell time models (RIFTA, RISE and UDO) and the proposed unified framework.

Method	Sampling	Optimization	Hyper parameters	Closed-form
RIFTA [14]	Regular	Nelder-Mead	Threshold α	✗
RISE [15]	Regular	Nelder-Mead	Threshold α	✗
UDO [21]	Arbitrary	Pattern Search	Proportionality β	✗
CUDO	**Arbitrary**	**None**	**None** (n = 1 is sufficient)	✓

3.2. Polynomial parameterization of dwell time

We begin by formulating the dwell time as a parametric function of the desired removal. In the matrix-form model, the relationship between the desired removal vector $\mathbf{z}_e \in \mathbb{R}^{N_z}$ and the dwell time vector $\mathbf{t} \in \mathbb{R}^{N_t}$ is given in Eq. (2). Rather than solving for $\mathbf{t}$ directly through inversion or iterative deconvolution, we express it as a nonlinear function of $\mathbf{z}_e$. Specifically, we utilize $\mathbf{R}^{\mathrm{T}} \in \mathbb{R}^{N_t \times N_z}$ to resample and interpolate the surface data onto the dwell positions. The dwell time vector is then modeled as a pointwise polynomial expansion in the resampled grid:

$$\mathbf{t} = \sum_{i=0}^{n} \gamma_i \left(\mathbf{R}^{\mathrm{T}} \mathbf{z}_e \right)^i, \tag{7}$$

where $\gamma_i \in \mathbb{R}$ are scalar coefficients and $(\cdot)^i$ denotes the element wise i-th power.

Optics EXPRESS

Substituting Eq. (7) into the convolution model yields the predicted removal:

$$\bar{\mathbf{z}} = \sum_{i=0}^{n} \gamma_i \mathbf{R} \left(\mathbf{R}^T \mathbf{z}_e\right)^i .$$

Let $\mathbf{\Phi} \in \mathbb{R}^{N_z \times (n+1)}$ be the basis matrix with columns $\boldsymbol{\phi}_i = \mathbf{R}\left(\mathbf{R}^T \mathbf{z}_e\right)^i$. Let $\mathbf{W} \in \mathbb{R}^{N_z \times N_z}$ be a diagonal binary matrix that masks the clear aperture, where $\mathbf{W}_{ii} = 1$ indicates locations inside the clear aperture and 0 elsewhere. Incorporating this mask, the optimal coefficients $\hat{\boldsymbol{\gamma}} = [\hat{\gamma}_0, \hat{\gamma}_1, \ldots, \hat{\gamma}_n]^T$ are obtained by minimizing the residual error in the clear aperture:

$$\begin{aligned} \hat{\boldsymbol{\gamma}} &= \min_{\boldsymbol{\gamma}} \|\mathbf{W}\left(\mathbf{z}_e - \bar{\mathbf{z}}\right)\|_2^2 \\ &= \min_{\boldsymbol{\gamma}} \|\mathbf{W}\left(\mathbf{z}_e - \mathbf{\Phi}\boldsymbol{\gamma}\right)\|_2^2 . \end{aligned} \tag{8}$$

The closed-form solution is then given by:

$$\boldsymbol{\gamma} = \left(\mathbf{\Phi}^T \mathbf{W}^T \mathbf{W} \mathbf{\Phi}\right)^{-1} \mathbf{\Phi}^T \mathbf{W}^T \mathbf{W} \mathbf{z}_e. \tag{9}$$

Since $\mathbf{W}$ is diagonal and symmetric, we have $\mathbf{W}^{\mathrm{T}}\mathbf{W} = \mathbf{W}$, which simplifies the expression to:

$$\boldsymbol{\gamma} = \left(\mathbf{\Phi}^T \mathbf{W} \mathbf{\Phi}\right)^{-1} \mathbf{\Phi}^T \mathbf{W} \mathbf{z}_e. \tag{10}$$

This windowed formulation ensures that the estimated dwell time polynomial best fits the surface shape only within the clear aperture, utilizing the same strategy in RIFTA, RISE and UDO and aligning with practical fabrication constraints.

3.3. Function-form model as a special case

When the surface and dwell grids coincide, the resampling matrix $\mathbf{R}^{\mathrm{T}}$ becomes the identity matrix, and Eq. (7) simplifies to

$$t(\mathbf{x}_j) = \sum_{i=0}^{n} \gamma_i \cdot z_e^i(\mathbf{x}_j). \tag{11}$$

The predicted removal is calculated as

$$\bar{z}\left(\mathbf{x}_j\right) = \sum_{i=0}^{n} \gamma_i \cdot \left[\mathrm{TIF} * (z_e)^i\right] \left[\mathbf{x}_j\right] .$$

The columns of the basis matrix $\mathbf{\Phi}$ are now given by $\boldsymbol{\phi}_i = \mathrm{TIF} * (z_e)^i$.

To restrict the optimization to the clear aperture, we again introduce a binary mask matrix $\mathbf{W} \in \mathbb{R}^{M \times N}$, where $M \times N = N_z$. The optimal coefficients $\hat{\boldsymbol{\gamma}}$ are obtained by minimizing the residual error in the clear aperture :

$$\begin{aligned} \hat{\boldsymbol{\gamma}} &= \min_{\boldsymbol{\gamma}} \|\mathbf{W} \cdot \left(z_e - \bar{z}\right)\|_2^2 \\ &= \min_{\boldsymbol{\gamma}} \|\mathbf{W} \cdot \left(z_e - \mathbf{\Phi}\boldsymbol{\gamma}\right)\|_2^2 . \end{aligned} \tag{12}$$

Let's define the clear-aperture counterparts of z_e and $\mathbf{\Phi}$ as $\tilde{z}_e = \mathbf{W} \cdot z_e$ and $\tilde{\mathbf{\Phi}} = \mathbf{W} \cdot \Phi$, respectively, the least-squares problem reduces to:

$$\hat{\boldsymbol{\gamma}} = \min_{\boldsymbol{\gamma}} \left\|\tilde{z}_e - \tilde{\mathbf{\Phi}}\boldsymbol{\gamma}\right\|_2^2 ,$$

Optics EXPRESS

which can be solved as

$$\boldsymbol{\gamma} = \left(\tilde{\boldsymbol{\Phi}}^T \tilde{\boldsymbol{\Phi}}\right)^{-1} \tilde{\boldsymbol{\Phi}}^T \tilde{z}_e. \tag{13}$$

This special case recovers the structure of RIFTA and RISE within the same closed-form framework. Unlike those methods, however, the current formulation does not require frequency-domain filtering and iterative threshold tuning.

3.4. Theoretical implications and interpretability

In dwell time optimization, the objective is to find the dwell time $\mathbf{t}$ that minimizes $\|\mathbf{z}_e - \mathbf{B}\mathbf{t}\|_2^2$. CUDO does not directly optimize $\mathbf{t}$. Instead, the polynomial parameterization introduces a smooth and physically interpretable model for dwell time estimation in CCOS. By expressing the dwell time $\mathbf{t}$ as a polynomial function of the surface shape $\mathbf{z}_e$ resampled to the dwell positions, as shown in Eq. (7), the method achieves three desirable theoretical properties: (1) global smoothness, (2) noise robustness, and (3) universality of approximation. These are supported by the following analysis.

The dwell time $\mathbf{t}$ modeled in Eq. (7) is equivalent to evaluating a scalar polynomial at each entry of $\mathbf{B}^{\mathrm{T}}\mathbf{z}_e$, imposing smoothness in the functional sense: each dwell time value is a continuous, differentiable function of the local surface height, which naturally suppresses high-frequency noise and sharp variations.

Furthermore, this model is interpretable in terms of physically meaningful quantities. The constant term γ_0 corresponds to uniform dwell time distribution, while higher-order terms introduce sensitivity to local error magnitude and nonlinear correction behavior. This polynomial expansion provides a low-dimensional parameterization that is easy to analyze, tune, or constrain.

Since $\mathbf{B}^{\mathrm{T}}\mathbf{z}_e$ is bounded on a finite domain, by applying the Weierstrass Approximation Theorem [24], we can derive a proposition that formalizes the approximation capacity of the model

Proposition 1 *Let $f : \mathbb{R} \to \mathbb{R}$ be a continuous mapping from the local (resampled) surface error to the corresponding dwell time at each dwell position. Then for any $\epsilon>0$, there exists a polynomial $P(x) = \sum_{i=0}^{n} \gamma_i x^i$ such that for all dwell time coordinates $\mathbf{u}_j$,*

$$\left| f\left(\left(\mathbf{B}^{\mathrm{T}}\mathbf{z}_e\right)_j\right) - P\left(\left(\mathbf{B}^{\mathrm{T}}\mathbf{z}_e\right)_j\right)\right| < \epsilon.$$

This result justifies the choice of a polynomial model: it is expressive enough to approximate any continuous dwell-removal relationship to arbitrary precision. Furthermore, the least-squares fitting procedure projects the desired removal profile onto the span of these polynomial basis functions convolved with the TIF, ensuring optimality in the l_2 norm within the clear aperture. Also, incorporating the clear-aperture mask $\mathbf{W}$ directly into the least-squares system guarantees that only physically realizable regions contribute to the estimation, avoiding spurious fitting outside the effective area. The proposed closed-form framework is theoretically robust, interpretable, and practically robust. It ensures:

- **Smoothness**, by construction through polynomials;
- **Noise suppression**, via dimensionality reduction and clear-aperture fitting;
- **Generalizability**, by unifying previous iterative methods as special cases and supporting arbitrary tool paths and sampling grids;
- **Analytical resolvability**, through least-squares regression in a carefully designed basis.

Optics EXPRESS

4. Comparative studies with the prior art

This section presents comparative studies between CUDO and three representative iterative methods: RIFTA, RISE, and UDO [10]. For a fair evaluation, the closed-form solver is directly substituted into each method, enabling side-by-side comparisons with their original counterparts.

4.1. Simulation setup

To quantify the accuracy, processing and computation efficiency, and robustness of the proposed closed-form solution, we replace the direct-search-based dwell time solvers in RIFTA, RISE, and UDO with the closed-form solver, resulting in "RIFTA with Closed-Form Solver", "RISE with Closed-Form Solver", and "UDO with Closed-Form Solver". The same synthetic surface topography used in a prior review of dwell time optimization methods [10] is adopted.

As shown in Fig. 1(a), the ground-truth dwell time $t_{GT}(x)$ is synthesized using the first 144 Chebyshev polynomials. The spatial resolution is set to 0.36 mm, and the size of $t_{GT}(x)$ is 20 mm × 190 mm, yielding 56 × 525 = 29,400 dwell points. Due to IBF machine dynamics [9], a minimum dwell time of Δt = 1.4 ms is added to each point to account for the nonzero dwell time constraint.

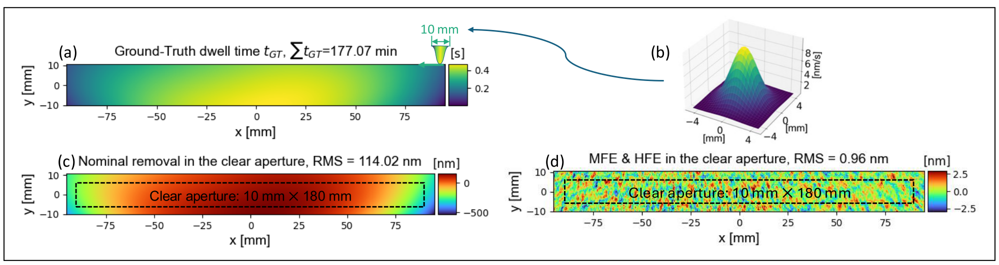

Fig. 1. Simulation framework and test cases: (a) Ground-truth dwell time $t_{GT}(x)$ synthesized from the first 144 Chebyshev polynomials, with 0.36 mm pixel size over a 20 mm × 190 mm grid (29,400 points) and a minimum dwell time offset Δt = 1.4 ms. (b) Gaussian TIF (σ = 1.6 mm, PRR = 10 nm/s). (c) Nominal target removal derived from $t_{GT}(x)$ and TIF. (d) MFE and HFE extracted from a pitch-polished flat mirror using a high-pass Gaussian filter (cut-off: 10 mm). Residuals are compared within the clear aperture (10 mm × 180 mm), with the calculation domain extended by one TIF radius to suppress edge effects.

A Gaussian Tool Influence Function (TIF) with standard deviation σ = 1.6 mm and Peak Removal Rate (PRR) of 10 nm/s, shown in Fig. 1(b), is convolved with $t_{GT}(x)$ to generate the nominal target removal map in Fig. 1(c). Under ideal conditions, this removal profile can be perfectly achieved by $t_{GT}(x)$. Dwell time solutions obtained form different optimization methods are compared directly against $t_{GT}(x)$. To evaluate robustness, Middle-Frequency Error (MFE) and High-Frequency Error (HFE) components, as shown in Fig. 1(d), are added to the nominal target removal. These components are extracted from a pitch-polished flat mirror using a high-pass Gaussian filter with a cut-off wavelength of 10 mm, indicating that they can hardly be corrected by this TIF.

To mitigate edge effects, the calculation domain is extended beyond the clear aperture by a margin equal to the TIF radius, though residual errors are evaluated only within the clear aperture. As RIFTA, RISE and UDO iteratively minimize the total dwell time [10], they are run until the absolute RMS difference between two consecutive iterations is less than 0.01 nm. All tests were performed on a workstation equipped with dual Intel Xeon Gold 5118 CPUs (12 cores per processor, 2.30 GHz) and 256 GB RAM.

4.2. Simulation result

Figure 2 compares dwell time maps obtained with the original RIFTA, RISE, and UDO methods (Figs. 2(a), 2(c), and 2(e)) against their counterparts using the proposed closed-form solver (Figs. 2(b), 2(d), and 2(f)), with the polynomial order fixed at $n = 1$. For each case, the total dwell time and the residual error maps are shown, allowing a direct comparison of process efficiency and residual surface quality between the iterative solvers and the closed-form approach. Note that the colorbar ranges for the residual error maps in the clear aperture are uniformly set to $\pm 3\sigma$, where σ is the standard deviation of the corresponding residual error, to better visualize detailed spatial patterns. The reported PV values in the figure titles correspond to the full range within the clear aperture. Across all three methods, the closed-form solver achieved the same or lower residual errors in the clear aperture while requiring shorter total dwell times, indicating a more effective minimization process. Among them, as shown in Figs. 2(e) and 2(f), UDO with the Closed-Form Solver yielded the smallest residual error (PV = 7.73 nm, RMS = 0.62 nm), consistent with the conclusion in [10] that UDO provides superior error suppression when properly optimized.

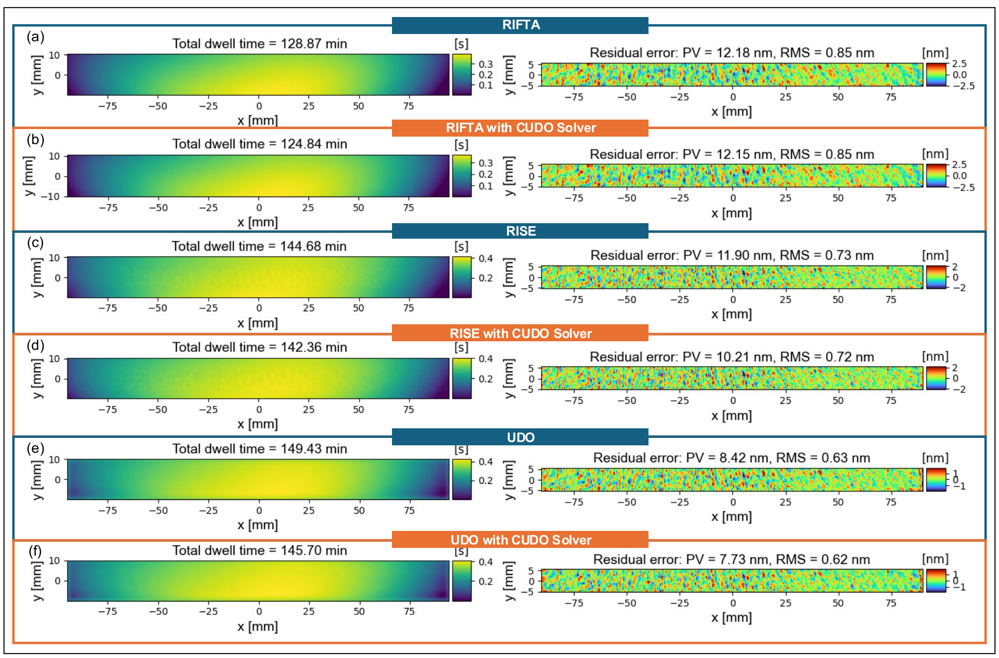

Fig. 2. Dwell time solution and estimated residual error calculated using (a) RIFTA, (b) RIFTA with CUDO Solver, (c) RISE, (d) RISE with CUDO Solver, (e) UDO, and (f) UDO with CUDO Solver. Methods using CUDO consistently achieve better accuracy and lower total dwell time compared to their original direct-search-based solvers.

Figure 3(a) further summarizes the trade-offs among total dwell time, residual RMS error, and computation time for all six methods. The x–y axes plot total dwell time against residual RMS error, with marker sizes indicating computation time. An inset bar chart provides a direct comparison of computation times across methods. The shaded region denotes the ground-truth dwell time versus residual error. Consistent with the previous conclusion [10], all six methods outperform the ground truth, achieving lower residual errors with shorter total dwell times. Notably, the closed-form methods (orange circles) not only match or improve accuracy but also

Optics EXPRESS

substantially reduce computation time, as clearly illustrated in both the marker sizes and the inset bar chart.

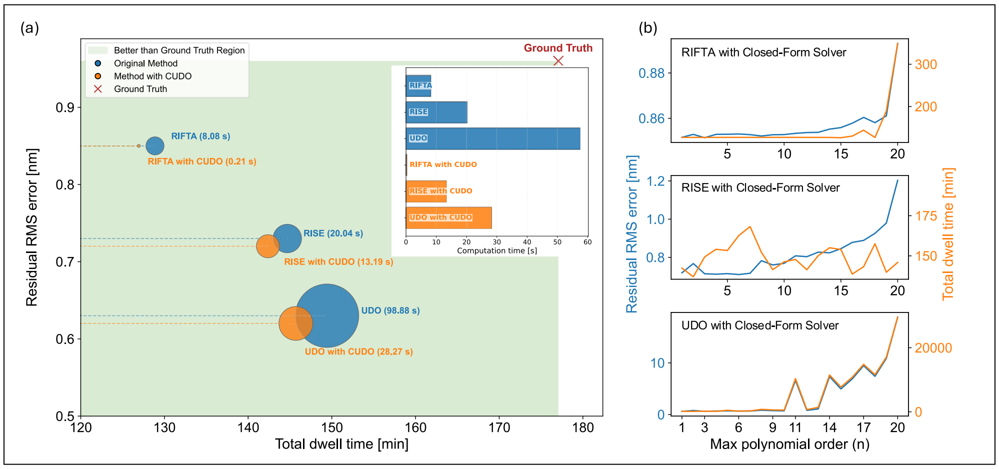

Fig. 3. (a) Trade-off among residual RMS error, total dwell time, and computation time for six methods (RIFTA, RISE, UDO, and their CUDO-solver-based counterparts). Marker size and inset represent computation time; shaded region denotes the ground-truth dwell time vs. residual error. CUDO achieve comparable or lower residuals with significantly reduced computation times. (b) Dependence of residual RMS error and total dwell time on the maximum polynomial order $n \in [1-20]$ for RIFTA, RISE, and UDO with the CUDO solver. The results show that $n = 1$ achieves the best trade-off between accuracy and processing efficiency.

In particular, because no iterative surface extension is performed in RIFTA, its runtime decreases from 8.08 s to 0.21 s. When measurement data reliably extends beyond the clear aperture, RIFTA with the closed-form solver provides the fastest and most favorable trade-off. Also, the computation time of the matrix-form method, UDO, is improved substantially. Whereas the original direct-search solver requires repeated matrix–matrix and matrix–vector multiplications across iterations, the closed-form approach eliminates these iterative operations, yielding an analytical solution in a single step. This reduction highlights one of the most significant advantages of the proposed framework, especially for matrix-form problems where computational burden is typically high.

Finally, Fig. 3(b) investigates the influence of the maximum polynomial order n (ranging from 1 to 20) on the performance of RIFTA, RISE, and UDO with the closed-form solver. For both RIFTA and UDO, increasing n leads to a monotonic increase in residual RMS error as well as total dwell time, indicating overfitting and reduced processing efficiency at higher polynomial orders. In contrast, RISE exhibits a steady increase in residual error with n, while its total dwell time oscillates around 150 min without a clear trend. These results confirm that $n = 1$ provides the best balance between accuracy and efficiency across all three methods, making higher-order expansions unnecessary in practice.

5. Experimental verification

To verify CUDO's applicability in practical fabrication tasks, we used it to finish a flat grating blank substrate. As shown in Fig. 4(a), the received substrate ($L \times W \times D = 220 \times 60 \times 60$ mm) was required to meet specifications of residual RMS height and slope errors are <1 nm and <0.2 μrad, respectively. However, measurements taken with our stitching interferometer

Optics EXPRESS

[25] revealed that all residual height, slope x and slope y errors all exceeded the specified limits (Figs. 4(b)–4(d)). Therefore, we decided to use our IBF system [9] to correct the residual errors.

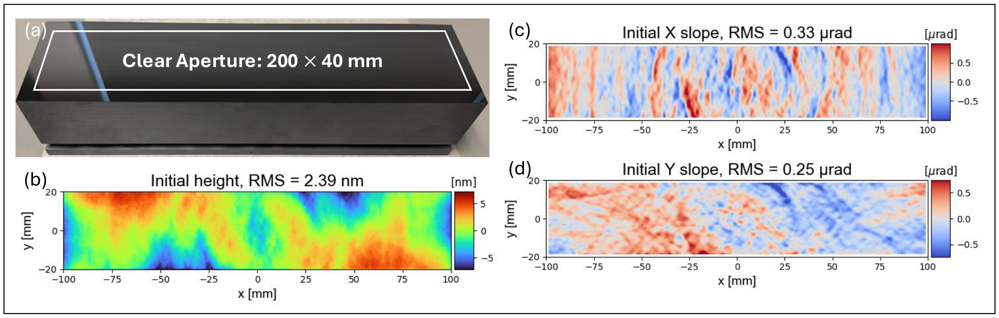

Fig. 4. Experimental substrate and pre-correction metrology used to validate CUDO on a practical IBF task. (a) Flat grating blank substrate ($L \times W \times D = 220 \times 60 \times 60$ mm) and specification: residual RMS height <1 nm and residual RMS slopes in x and y each <0.2 μrad within the clear aperture. (b)-(d) As-received measurements from our stitching interferometer [25]: residual height (nm), slope-x, and slope-y (μrad) maps, all exceeding the specification and motivating correction using our IBF system [9].

In the IBF process, a KDC10 ion source was operated at a beam voltage of 600 V, beam current of 10 mA, and accelerator voltage of −90 V. A ϕ5 mm diaphragm was placed in front of the source, yielding an approximately Gaussian TIF with a $3\sigma = 5$ mm and a Peak Removal Rate (PRR) of 6.8 nm/s. We applied RISE with CUDO to calculate dwell time using the height error map shown in Fig. 4(a), since the clear aperture shape is rectangular. The resulting dwell time distribution is shown in Fig. 5(a), and the corresponding estimated post-IBF height and slope maps are shown in Figs. 5(b)–5(d). For a single correction cycle of 20.89 min, the predicted residual RMS height and slopes are 0.22 nm, 0.13 μrad and 0.08 μrad, respectively, all meeting the specification.

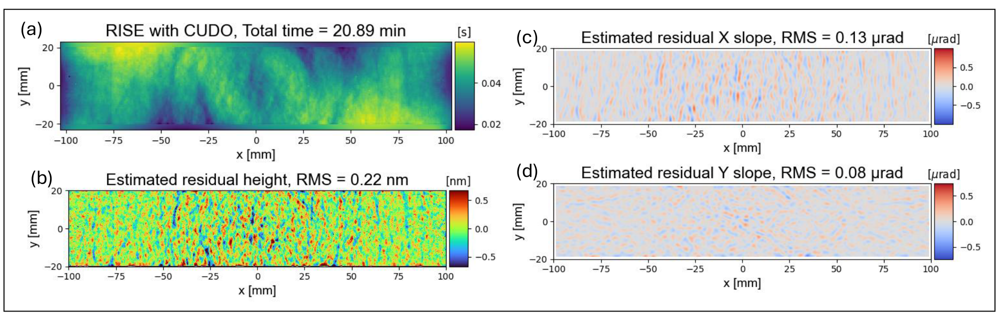

Fig. 5. RISE+CUDO simulation for the grating substrate using the measured height error (Fig. 4(b)) and a Gaussian TIF ($3\sigma = 5$ mm, $PRR = 6.8$ nm/s). (a) Computed dwell time map. (b) Estimated residual height. (c),(d) Estimated residual slopes in x and y. For a 20.89 min IBF cycle, the predicted residual RMS values are 0.22 nm, 0.13 μrad, and 0.08 μrad, satisfying the specified limits.

After executing the RISE+UDO dwell time, the post-IBF measured residual maps are shown in Fig. 6. Within the clear aperture, the residual RMS values are 0.37 nm for height (Fig. 6(a)), 0.15 μrad for slope-x (Fig. 6(b)), and 0.09 μrad for slope-y (Fig. 6(c)). All three meet the specification (height < 1 nm; slopes < 0.2 μrad). The spatial patterns in the slope maps are consistent with the predicted post-IBF maps (Figs. 5(c) and 5(d)). The small low-frequency discrepancy in the height maps (Fig. 6(b) vs. Fig. 5(b)) is attributed to a slight underestimation ($\approx 9\%$) of the TIF removal rate. A subsequent IBF run incorporating this corrected TIF would be expected to further reduce the residual height error toward the predicted limit. Nevertheless, as the achieved values already met all specifications, no additional correction was performed.

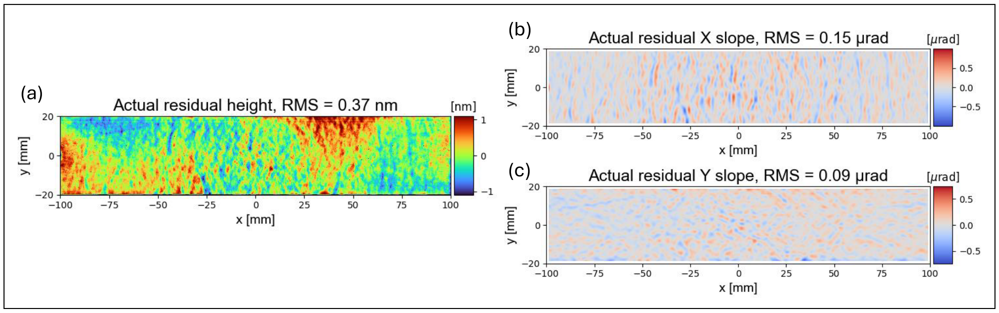

Fig. 6. Post-IBF metrology of the grating blank substrate after one 20.89 min RISE+CUDO correction: (a) measured residual height, (b) residual slope-x, and (c) residual slope-y. RMS values within the clear aperture are 0.37 nm, 0.15 μrad, and 0.09 μrad, respectively, each satisfying the specification (height < 1 nm; slopes < 0.2 μrad)

6. Discussion

The comparative studies presented in Section 4 highlight several important implications of the CUDO framework. The results confirm that the closed-form solver consistently matches or outperforms iterative counterparts in terms of residual error while substantially reducing computation time. This efficiency gain eliminates the need for iterative thresholding or parameter searches, thereby enhancing automation and scalability for large-aperture optical fabrication.

6.1. Trends with polynomial order n

Figure 3(b) investigates performance as the maximum polynomial order n increases. Two distinct patterns emerge. (i) Residual RMS: the increase is marginal in RIFTA, moderate for RISE, and substantial for UDO at large n. (ii) Total dwell time: RFITA and UDO show an almost monotonic growth with n, whereas RISE exhibits an oscillatory dwell-time trend.

These behaviors are explained by how higher-order bases interact with the iterative algorithmic loop used in practice. Although the coefficients $\boldsymbol{\gamma}$ are estimated by a clear-aperture least-squares fit within the CUDO framework (Eqs. (7)–(10)), RIFTA, RISE, and UDO are executed iteratively with two constraints enforced at each iteration: (i) minimum dwell time adjustment ($t<\Delta t \Rightarrow \Delta t$) and (ii) total-dwell-time minimization before resolving. As n increases, the basis $\mathbf{\Phi}$ constructed from powers of the resampled field becomes more collinear, making $\mathbf{\Phi}^T\mathbf{W}\mathbf{\Phi}$ increasingly ill-conditioned, amplifying coefficient variance. The resulting $\mathbf{t}$ fields are clipped and shrunk, so the realized removal deviates from the unconstrained fit, raising realized residual RMS and total dwell time even though the in-model least-squares error would not. In other words, the observed degradation at high n is best described as variance amplification under ill-conditioning, coupled with per-iteration constraints and dwell time minimization.

6.2. Why RISE dwell time oscillates; why UDO grows fastest

Both RISE and UDO employ surface extension to mitigate edge effects. In RISE (function-form on a regular grid), the extension behaves as an implicit boundary regularizer that reduces edge gain. Its interaction with the polynomial parameterization can intermittently lower the amount of compensatory valid dwell time required after clipping at certain n, producing the observed non-monotonic dwell time trend.

By contrast, UDO uses a matrix-form mapping in which the polynomial is built on the resampled field $\mathbf{R}^T\mathbf{z}_e$ (rather than $\mathbf{z}_e$ on a regular grid). This resampling introduces additional volatility (interpolation and non-uniform path density) and strengthens inter-column correlations in $\mathbf{\Phi} = \left[\mathbf{R}\left(\mathbf{R}^T\mathbf{z}_e\right)^0, \mathbf{R}\left(\mathbf{R}^T\mathbf{z}_e\right)^1, \ldots\right]$. As n grows, pointwise powers $\left(\mathbf{R}^T\mathbf{z}_e\right)^i$ accentuate extremes, and the forward operator $\mathbf{R}\mathbf{R}^T$ can further boost certain spatial components, so the variance-constraints interaction is most severe for UDO, explaining its faster RMS growth and very large dwell times at high n.

6.3. Why $n = 1$ is sufficient

The CUDO framework supports nonlinear mappings (Eq. (7)), but the CCOS regime considered in this study are well described by $n = 1$. Two facts justify this choice. First, with a fixed TIF, the forward removal model (convolution) is linear, so the dominant nonlinearity in practice arises from the algorithmic loop (minimum dwell time enforced and per-iteration total dwell time minimization) rather than from the instantaneous $\mathbf{t}$-$\mathbf{z}_e$ law within a single solve. Second, increasing n primarily inflates variance (Section 6.1), which degrades the realized residual and efficiency once constraints are enforced. Empirically, as shown in Fig. 3(b), $n = 1$ yields the best accuracy-efficiency trade-off across all three methods. This is consistent with the linear assumption in UDO ($\mathbf{t} = \beta\mathbf{R}^T\mathbf{z}_e$), which can be treated as a special case in the CUDO framework.

7. Conclusion

This work introduced CUDO, a Closed-form Universal Dwell-time Optimization framework that analytically improves three state-of-the-art iterative methods: Robust Iterative Fourier Transform-based Algorithm (RIFTA), Robust Iterative Surface Extension (RISE), and Universal Dwell time Optimization (UDO). By reformulating dwell time estimation as a polynomial regression problem, the framework provides direct analytical solutions that eliminate iterative optimization and hyperparameter tuning.

Simulation studies demonstrated that the closed-form solver consistently achieves comparable or lower residual errors than its iterative counterparts while drastically reducing computation time. The results further confirm that a first-order polynomial ($n = 1$) is sufficient for practical applications, offering an optimal balance between accuracy and process efficiency. Tests under middle- and high-frequency error, as well as measurement noise, showed that the closed-form solver maintains stability and avoids overfitting, with UDO in its closed-form variant delivering the best overall accuracy.

CUDO not only unifies function-form and matrix-form dwell time models but also establishes a scalable and robust foundation for real-time and large-aperture optical fabrication. Future work will focus on extending this framework to multi-tool and adaptive tool path scenarios, as well as integrating it into in-situ fabrication and metrology systems.

Funding. Office of Science (DE-SC0012704); U.S. Department of Energy (FWP-PS044); Brookhaven National Laboratory (BNL LDRD 25-024).

Disclosures. The authors declare no conflicts of interest.

Data availability. Data underlying the results presented in this paper are not publicly available at this time but may be obtained from the authors upon reasonable request. An implementation of RIFTA for reference and reproducibility is openly available at [26].

References

1. M. Ghigo, G. Vecchi, S. Basso, *et al.*, “Ion figuring of large prototype mirror segments for the E-ELT,” in *Advances in Optical and Mechanical Technologies for Telescopes and Instrumentation*, vol. 9151 R. Navarro, C. R. Cunningham, and A. A. Barto, eds., International Society for Optics and Photonics (SPIE, 2014), p. 91510Q.

2. D. Kim, H. Choi, T. Brendel, *et al.*, "Advances in optical engineering for future telescopes," Opto-Electron. Adv. **4**(6), 210040 (2021).
3. M. Weiser, "Ion beam figuring for lithography optics," Nucl. Instrum. Methods Phys. Res., Sect. B **267**(8-9), 1390–1393 (2009).
4. J. E. E. Baglin, "Ion beam nanoscale fabrication and lithography—a review," Appl. Surf. Sci. **258**(9), 4103–4111 (2012).
5. J. Yamada, S. Matsuyama, R. Hirose, *et al.*, "Compact full-field hard x-ray microscope based on advanced kirkpatrick–baez mirrors," Optica **7**(4), 367–370 (2020).
6. J. Yamada, S. Matsuyama, I. Inoue, *et al.*, "Extreme focusing of hard X-ray free-electron laser pulses enables 7 nm focus width and 10^{22} W cm^{-2} intensity," Nat. Photonics **18**(7), 685–690 (2024).
7. W.-L. Zhu and A. Beaucamp, "Compliant grinding and polishing: A review," International J. Machine Tools and Manufact. **158**, 103634 (2020).
8. X. Ke, Y. Yu, K. Li, *et al.*, "Review on robot-assisted polishing: Status and future trends," Robotics Computer-Integrated Manufact. **80**, 102482 (2023).
9. T. Wang, L. Huang, Y. Zhu, *et al.*, "Development of a position-velocity-time-modulated two-dimensional ion beam figuring system for synchrotron x-ray mirror fabrication," Appl. Opt. **59**(11), 3306–3314 (2020).
10. T. Wang, X. Ke, L. Huang, *et al.*, "A comprehensive review of dwell time optimization methods in computer-controlled optical surfacing," Light: Adv. Manufact. **5**(3), 1 (2024).
11. R. A. Jones, "Optimization of computer controlled polishing," Appl. Opt. **16**(1), 218–224 (1977).
12. S. R. Wilson and J. R. McNeil, "Neutral ion beam figuring of large optical surfaces," in *Workshop on Optical Fabrication and Testing* (Optica Publishing Group, 1987), paper FAA4.
13. C. J. Jiao, S. Y. Li, and X. H. Xie, "Algorithm for ion beam figuring of low-gradient mirrors," Appl. Opt. **48**(21), 4090–4096 (2009).
14. T. Wang, L. Huang, H. Kang, *et al.*, "RIFTA: A Robust Iterative Fourier Transform-based dwell time Algorithm for ultra-precision ion beam figuring of synchrotron mirrors," Sci. Rep. **10**(1), 8135 (2020).
15. T. Wang, L. Huang, H. Choi, *et al.*, "RISE: robust iterative surface extension for sub-nanometer X-ray mirror fabrication," Opt. Express **29**(10), 15114–15132 (2021).
16. C. L. Carnal, C. M. Egert, and K. W. Hylton, "Advanced matrix-based algorithm for ion-beam milling of optical components," in *Current Developments in Optical Design and Optical Engineering II*, vol. 1752 R. E. Fischer and W. J. Smith, eds., International Society for Optics and Photonics (SPIE, 1992), pp. 54–62.
17. L. Zhou, Y. Dai, X. Xie, *et al.*, "Model and method to determine dwell time in ion beam figuring," Nanotechnology and Precision Engineering **5**(2), 107–112 (2007).
18. J. F. Wu, Z. W. Lu, H. X. Zhang, *et al.*, "Dwell time algorithm in ion beam figuring," Appl. Opt. **48**(20), 3930–3937 (2009).
19. T. Y. Wang, L. Huang, M. Vescovi, *et al.*, "Study on an effective one-dimensional ion-beam figuring method," Opt. Express **27**(11), 15368–15381 (2019).
20. H. Kang, T. Wang, H. Choi, *et al.*, "Genetic algorithm-powered non-sequential dwell time optimization for large optics fabrication," Opt. Express **30**(10), 16442–16458 (2022).
21. T. Wang, L. Huang, M. Vescovi, *et al.*, "Universal dwell time optimization for deterministic optics fabrication," Opt. Express **29**(23), 38737–38757 (2021).
22. V. S. Negi, T. Wang, H. Garg, *et al.*, "Random adaptive tool path for zonal optics fabrication," Opt. Express **30**(16), 29295–29309 (2022).
23. X. Ke, T. Wang, H. Choi, *et al.*, "Dual-tool multiplexing model of parallel computer controlled optical surfacing," Opt. Lett. **45**(23), 6426–6429 (2020).
24. K. Weierstrass, "Über die analytische darstellbarkeit sogenannter willkürlicher functionen einer reellen veränderlichen," Sitzungsberichte der Königlich Preussischen Akademie der Wissenschaften zu Berlin pp. 633–639, 789–805 (1885).
25. L. Huang, T. Wang, K. Tayabaly, *et al.*, "Stitching interferometry for synchrotron mirror metrology at national synchrotron light source ii (nsls-ii)," Opt. Lasers Eng. **124**, 105795 (2020).
26. T. Wang and Y. Ma, "RIFTA," GitHub (2020), https://github.com/TWANG006/RIFTA.git.